[SSC25-RAI-09]

A Radio Payload for In-Space Sub-Terahertz Communications

Andrew Benincasa, Sergi Aliaga, Albert Diez-Comas, Josep Miquel Jornet
Northeastern University
360 Huntington Ave, Boston, MA 02115;
benincasa.an@northeastern.edu

ABSTRACT

This paper presents the first fully integrated design of a CubeSat-compatible sub-terahertz (sub-THz) radio payload for in-space communications at 225 GHz. Addressing the growing congestion in traditional RF bands and the limitations of Free Space Optical systems, the proposed system leverages recent breakthroughs in compact high-frequency front-ends, horn antenna arrays, and RFSoC-based digital processing to unlock multi-GHz bandwidths in the underutilized sub-THz spectrum. A detailed feasibility study confirms link closure from low Earth orbit using state-of-the-art components, and the payload's architecture is engineered for real-time high-speed uplink/downlink under stringent CubeSat size, weight, and power (SWaP) constraints. The proposed payload will fly aboard the TeraLink CubeSat mission, marking a critical step toward operational sub-THz satellite links and ushering in a new era of broadband, high-frequency space communications.

1 INTRODUCTION

In recent years, space-based communications and networking have undergone a fundamental transformation. What began with transmitting low-resolution images in the post-Apollo era has now evolved into distributed satellite networks supporting global internet connectivity. This is marked by the deployment of multiple low-Earth orbit (LEO) constellations of small satellites by government agencies like the U.S. Space Force (USSF)[1] and the U.S. Air Force (USAF),[2] as well as private efforts such as Starlink and Project Kuiper. These constellations aim to shape the future of both near-Earth and deep-space communication. However, their success, which requires broadband access links (uplink (UL) and downlink (DL)) and cross-links (or inter-satellite links (ISLs)) with each satellite,[3] relies heavily on fast and secure communication payloads, which are not always guaranteed due to tight size, weight, and power (SWaP) requirements and/or spectrum scarcity.

Furthermore, a growing interest in human exploration of the cislunar environment, the lunar south pole, and Mars over the next decade[4–6] is driving the creation of new planetary science and deep space exploration instruments.[7–9] These advanced instruments, designed for high-resolution imaging, increased scientific data production, and potentially even video streaming, also require significantly higher data rates to stream the captured data back to Earth and, thus, achieve mission success.

This exponentially growing number of science missions and massive satellite constellation deployments is straining current space communication methods both in terms of reliability and performance. As a result, major infrastructures are already facing limitations and challenges. Early efforts by major satellite partnerships like Apple-Globalstar and Qualcomm-Iridium are limited to low data-rate applications such as SOS text messages[10] or a few Mbps data connectivity if using a fixed Very Small Aperture Terminal (VSAT),[11] while NASA's Deep Space Network (DSN) mid-2010s congestion predictions are becoming a reality.[12,13] Additionally, spectrum disputes among these service providers,[14] as well as concerns over the coexistence with Earth exploration services[15] have also arisen, mainly constrained by the limited spectrum below the Ka-band (< 40 GHz).

To meet these increasing demands, new communication and networking solutions for the next generation of space communication systems are being investigated.[16,17] In particular, Free Space Optical (FSO) communication, typically within the infrared spectrum (187 to 400 THz or, equivalently, 750 to 1600 nm), is being explored to improve satellite data rates.[18–20] The substantial bandwidth available at this very high frequency plays to its advantage and, presently, optical technology is more accessible and mature, offering promising possibilities.[21] However, notable physical challenges persist. For ISLs, thin laser-formed beams demand precise pointing, presenting a substantial hurdle.[22] For UL/DL, the chal-

lenge is even larger: strong dependence on atmospheric conditions becomes critical in signal propagation and reception (e.g., scattering from molecules and particles, turbulence-induced scintillation, and beam wandering), even in clear-sky conditions.[23] These challenges captivate the research community's attention, spurring ongoing innovation in this domain.[24–26]

Alongside FSO, communication in the subterahertz (sub-THz, 0.1–0.3 THz) and terahertz bands (THz, 0.3–10 THz), which offer multi-GHz portions of spectrum allocated to fixed, mobile, and satellite communications, is regarded as a key technology to enable unprecedented data rates in, from, and to space. In this direction, new architectures based on distributed LEO CubeSat networks leveraging these spectrum bands hold the potential to unlock the necessary breakthroughs in global secure high-rate connectivity. By solving the spectrum scarcity problem, conquering this frequency band will advance human space exploration of the Moon and beyond, provide direct support for natural disaster response, enable advanced climate change monitoring, and more.[27–29]

Sitting between the crowded radio frequency (RF) spectrum and optics, the THz band offers unique advantages over FSO communications while providing similar bandwidth and data rates. In UL/DL, state-of-the-art THz hardware can provide less constraining pointing requirements, with THz horn antennas capable of a 3 dB beamwidth in the range of 13° with minimal footprint.[30] Furthermore, the sub-THz band can offer better channel conditions with fewer losses compared to FSO, including more than 60 dB lower spreading loss, 100 dB lower clouds and rain attenuation, and negligible scattering and turbulence losses for LEO ULs and DLs. Furthermore, molecular absorption loss, one of the main concerns in (sub-)THz communication, can be minimized by adequately selecting specific carriers within the multi-GHz absorption-free bands present in the THz band.[31]

These present advantages over current and emerging satellite communications technologies position the THz band as a very promising alternative to support new advancements in space communications. Focusing on the sub-THz band as a pioneering step, major regulatory entities, like the Federal Communications Commission (FCC), are already allocating multiple portions of spectrum for both Earth-to-space and space-to-Earth communications, including the 123-130 GHz, 217-226 GHz, and 232-240 GHz bands.[32] As mentioned, these allocations are conveniently located within strategic absorption-free windows in the sub-THz band, making them all the more appealing for next-generation satellite communication systems.

Up until recently, the potential for THz in space remained theory, due to the lack of hardware compatible with space. However, thanks to the rapid advancement of THz technology, theoretical possibilities have been brought closer to realization, and the deployment of a space-based THz communications system is now possible. *This paper presents the first design of a sub-THz radio payload compatible with CubeSat SWaP constraints, enabling UL and DL access links in space at carrier frequencies near 225 GHz with data rates exceeding 100 Mbps.*

The remainder of the paper is organized as follows. In Section 2 we provide an in-depth review of the state-of-the-art THz and sub-THz hardware and highlight the optimal technological approaches for its deployment in space. We determine the feasibility of sub-THz links in space using such hardware capabilities in Section 3. In Section 4, we detail the payload design that can achieve such capabilities and provide a preliminary characterization of the payload components. Finally, in Section 5, we summarize the main characteristics of the designed radio and outline the planned steps to build the proposed design and to deploy it for flight qualification.

2 STATE-OF-THE-ART HARDWARE OVERVIEW

Over the past 15 years, THz communication has become a possibility through the progressive narrowing of the so-called "THz technology gap". Technological breakthroughs in all main radio components, mainly (1) antennas, (2) analog front-ends (mixers, amplifiers, etc.), and (3) digital signal processing (DSP) engines, have pioneered the first strides of THz communication.[33] As such, platforms packaging these elements in the form of transmitters and receivers capable of multi-GHz *terrestrial* point-to-point links at sub-THz and THz frequencies are now available.[34] In this section, we provide a comprehensive review of the state-of-the-art for each of these component categories and single out the best candidate approaches for the design of the first space-ready sub-THz radio.

Antennas

Antennas are fundamental components of any wireless communication system. Serving as the interface between guided electromagnetic waves and free-space electromagnetic radiation, they are broadly categorized into (1) omnidirectional antennas, which radiate energy uniformly in all directions

and are ideal for applications requiring wide area coverage; and (2) directional antennas, which focus the energy in a specific direction to improve gain, link margin, and overall communication range.

At sub-THz frequencies, the use of directional antennas becomes essential. Due to significant free-space path losses, omnidirectional antennas typically cannot provide sufficient gain for reliable communication. As the physical size of any antenna must be close to the wavelength of the desired resonant frequency, the small < 3 mm wavelength at sub-THz frequencies and beyond results in a very limited effective aperture and, consequently, minimal captured power. The effective aperture A of an antenna is related to its gain G and wavelength λ as described by the well-known relation:

$$A = \frac{\lambda^2}{4\pi} G. \tag{1}$$

For a fixed antenna size, as frequency increases (and wavelength decreases), even compact apertures can yield high gain, a crucial advantage for size-constrained satellite platforms like CubeSats. For instance, a 10×10 cm aperture (1U side) operating at 200 GHz ($\lambda = 1.5\ mm$) achieves roughly a gain of 47 dBi, much greater compared to the 21 dBi gain attainable at 10 GHz. At even lower frequencies, such as 3 GHz, the aperture size approaches the wavelength, causing antennas to approach omnidirectional behavior.

Thus, to close the sub-THz link budget at orbital distances, high-directivity antennas are essential.[35,36] *Parabolic reflectors* are commonly used in space applications due to their relatively large gain-to-aperture ratio. These systems use a feed element (usually a horn) to focus energy onto a parabolic dish, producing a narrow beam. However, due to their size and mechanical complexity, they are not suitable for small platforms like CubeSats.

Conversely, *horn antennas* by themselves represent a compact and efficient alternative for small satellites. Their directivity can be further enhanced using dielectric lenses, which focus the beam at the horn's aperture. For even more compact implementations, metasurfaces can be engineered to impart specific phase profiles, which can replicate the focusing behavior of lenses with thinner, lighter structures.[37]

Moreover, *antenna arrays*, that is, the combination of multiple identical antennas to achieve constructive interference in specific directions, provide another route to achieving high gain at sub-THz frequencies. Here, traditional substrate-based antenna arrays, such as microstrip patches, which are popular at microwave frequencies for their low profile and ease of integration, become significantly less practical at THz frequencies due to several limitations. High dielectric and conductor losses, miniaturized dimensions that make fabrication extremely sensitive to tolerances, and the requirement for a large number of elements to achieve sufficient gain, lead to complex and lossy feeding networks for sub-THz frequencies.[38] For this reason, the candidate technology for CubeSat antennas at such high frequencies is *arrayed horn antennas*. These combine the inherent directivity and low manufacturing complexity of horns with the arraying factor to achieve very high overall gain in compact footprints.[39,40]

Nonetheless, working at THz frequencies introduces several practical engineering challenges to these designs. As feature sizes in the horns approach the limits of modern machining capabilities, maintaining precise manufacturing tolerances becomes increasingly critical. These constraints not only affect performance but also drive up fabrication costs. At such small wavelengths, surface roughness and material finish are also significant factors, as even minute imperfections can adversely impact electromagnetic behavior. State-of-the-art precision machining can reliably achieve tolerances on the order of tens of micrometers and fabricate features down to a few hundred micrometers. With careful design considerations, this level of precision is sufficient for many sub-THz hardware applications.

When it comes to the materials utilized, gold plating is frequently used in space applications due to the absence of atmospheric oxygen, which eliminates the risk of oxidation. Gold offers excellent electrical conductivity, chemical inertness, and high reflectivity, all of which contribute to improved antenna efficiency. Notably, for prototyping or cost-sensitive applications, aluminum is a viable alternative due to its affordability, low machining complexity, and acceptable conductivity for many practical applications.

One paramount aspect of highly directional antennas is their alignment. Antennas with 40 dBi and 60 dBi gains (typical values in sub-THz link budgets) exhibit beamwidths of approximately 2° and 0.2°, respectively. Although challenging, alignment of such narrow beams is more manageable than in optical communication, where pencil-like beams reach micro radian ($\mu\text{rad} \approx 10^{-5\circ}$) scales. Typically, mechanical alignment is the most common solution in both space-to-ground and inter-satellite links. On the ground, parabolic antennas are often mounted on steerable platforms that physically tilt the an-

tenna toward the satellite. In space, attitude control systems, such as gyroscopes or reaction wheels, are used to ensure antenna alignment.

An alternative to mechanical steering is electronic beam steering, achieved through phased array antennas. At sub-THz frequencies, these antennas require complex chip designs due to the need for a larger number of densely packed elements compared to microwave arrays, with each element requiring individual feed control. To reduce this complexity, reconfigurable reflectarrays have been proposed as a viable alternative.[41] In these systems, phase control is offloaded to a passive reflecting surface, enabling fixed reconfigurability to be implemented off-chip.

Notably, both (sub-)THz phased arrays and reconfigurable reflectarrays face substantial challenges in space. The active components typically used in these systems, such as PIN diodes and varactors, suffer from frequency cutoff limitations and are increasingly affected by parasitic effects. These issues lead to considerable insertion losses, typically in the range of 10-20 dB,[38] significantly impacting their efficiency and scalability for practical high-frequency space applications.

Finally, polarization is another critical factor in high-frequency antenna designs. Linear polarization is susceptible to degradation caused by atmospheric effects, such as Faraday rotation and depolarization, as well as by misalignment between antennas. Consequently, circular polarization is often preferred, as it provides greater robustness in dynamic or lossy environments, such as space. Circularly polarized (sub-)THz antennas can be implemented directly, although they typically involve more complex designs. An alternative approach is to use linear-to-circular polarization converters. However, in small satellite platforms like CubeSats, linearly polarized antennas are often more practical due to constraints on size and complexity. Although this results in a 3 dB polarization mismatch loss when communicating with a circularly polarized counterpart, it is often an acceptable trade-off for simplifying the design and ensuring reliable communication.

In summary, sub-THz antennas for CubeSats must balance high gain, compact size, fabrication feasibility, and alignment precision. For this reason, linearly-polarized horn antennas and their arrayed derivations stand out as the best candidate technology for future spacecraft thanks to their low complexity manufacturing, surface roughness efficiency, and high performance.

Analog Front Ends

Analog front ends are a core component in any satellite radio, serving as the primary gateway to generate, modulate, filter, and amplify both outgoing and incoming signals. In them, three pathways exist for THz carrier frequency generation: intrinsic THz resonance (plasmonic approach), frequency down-conversion (photonic approach), and frequency up-conversion (electronic approach).[42]

The first, a nascent but emerging method, focuses on the intrinsic generation of THz frequencies through the excitation of plasma waves and the propagation of surface plasmon polariton (SPP) waves. Through the Dyakonov-Shur Instability, plasmonic terahertz sources utilize oscillations of electrons between asymmetric boundaries in 2-D electron gases (2DEGs) within high electron mobility transistors (HEMTs) to directly generate THz frequencies.[43] Plasmonic sources occupy an extremely small footprint, making them suitable for use in nanoscale applications. Despite their low power consumption, this form factor limits plasmonic sources to only around 1μW of output power.[44] Due to this, the plasmonic approach is neither viable nor well-suited for orbital link distances.

Conversely, the photonic approach consists of methods that down-convert optical signals to THz frequencies. Quantum Cascade Lasers (QCLs) are one of the main photonic technologies that can intrinsically radiate at the upper end of the terahertz band ($\sim$ 10 THz), reaching output powers in the range of tens to hundreds of milliwatts at cryogenically cooled temperatures. However, QCLs have stringent requirements to remain at these cold temperatures, as at room temperature, output power drops into the microwatt range.[45] Furthermore, only non-coherent modulation with limited bandwidth is possible with QCLs due to large transient times.[46] Another photonic option is laser multiplication, which is used to down-convert QCL optical signals into the sub-THz band. An example of this is frequency difference generation, which utilizes photomixers to combine two optical signals at different frequencies and radiate the difference of the two by filtering and amplifying the corresponding harmonic. The conversion losses of such a photomixer limit the output power to a few milliwatts and occupy a large footprint.[47] In other words, while respectable output power levels can be reached with this approach, it comes at a cost of system performance and SWaP. Presently, due to the additional costs of temperature regulation, this approach is incompatible with space-based applications.

Finally, in the electronic approach, THz oscilla-

tion is achieved by frequency up-conversion through various frequency multiplying stages. These frequency multiplying circuits are analogous to active RF mixers and can be implemented using various nonlinear devices, including transistors and micro-electromechanical systems.[42] Notably, the use of Schottky barrier diodes has been the most successful multiplier technology.[48] Pioneered at NASA's Jet Propulsion Laboratory (JPL), these multipliers showcased record-breaking output power levels and remain the dominant choice for electronic up-conversion.[49]

Concretely, output power levels in the sub-THz band range from 100 mW to almost 400 mW in systems developed by JPL, Virginia Diode, Inc. (VDI), and other groups. In the THz range, frequency up-conversion is also possible, albeit output power degrades below 100 mW down to microwatt levels, reducing the possible transmission distance.[42] A sub-THz design using this technology has been demonstrated to achieve multi-kilometer, multi-gigabit-per-second links,[50] paving the way for even longer link distances. Operating at 210-230 GHz with approximately 200 mW of output power, this sets an important precedent for frequency up-conversion as the primary candidate for an equivalent space-based sub-THz implementation.

Therefore, among the three approaches, the electronic approach through frequency up-conversion is the most promising alternative for enabling THz space communication. Proven hardware is capable of multi-kilometer multi-gigabit-per-second terrestrial links,[50] and recent advancements have pushed output power further beyond these feats and well above its photonic and plasmonic counterparts. Additionally, electronic-based sub-THz hardware is becoming increasingly more compact, with engineering models for a single front-end occupying around 1U of space.

Digital Signal Processing

At the heart of every radio lies a fundamental separation between the analog and digital domains, with DSP long recognized as more efficient, flexible, and adaptable than its analog counterpart. This boundary is defined by the data converters–namely, Analog-to-Digital converters (ADCs) and Digital-to-Analog converters (DACs)–whose sampling rate f_s remains their most critical figure of merit as it directly limits usable bandwidth. In recent years, advancements in electronic circuit design have enabled sampling rates to exceed 100 Gigasamples-per-second (GSps), thereby catalyzing the development of ultrabroadband processing platforms that can exploit the extensive bandwidth available in the THz band. Thanks to these breakthroughs, most contemporary ground-based THz testbeds can process ultrabroadband signals (tens of GHz and beyond).[51–56]

However, many of these platforms still rely on non-real-time signal processing–where signals are pre-generated at the transmitter and post-processed after storage at the receiver–and typically require bulky, high-end arbitrary arbitrary waveform generators (AWGs) and digital storage oscilloscopes (DSOs), which are impractical for flight-qualified systems. To address this limitation, cutting-edge THz communication testbeds such as the TeraNova platform at Northeastern University[33] have begun integrating novel DSP engines based on Radio Frequency System on Chip (RFSoC) architectures.[57] An RFSoC is a highly integrated solution that combines programmable logic (FPGA), high-speed data converters (ADCs/DACs), and a processing system (CPU/SoC) on a single chip. This architecture enables real-time reconfigurability for custom DSP and benefits from low-latency on-chip execution.[58,59]

While RFSoCs currently offer sampling rates on the order of 10 GSps, one of their key advantages is the ability to be embedded into compact support boards, often occupying footprints smaller than 1U. Thus, due to their exceptional performance-to-SWaP ratio, they are the preferred candidates for enabling high-speed THz communications in space.

3 FEASIBILITY STUDY

Considering the reviewed state-of-the-art hardware, this section outlines the requirements necessary for the design of the first sub-THz payload compatible with CubeSat SWaP requirements. We present an in-depth feasibility analysis of a sub-THz link between space and Earth to establish threshold markers and gauge performance capabilities. At orbital link distances ($>$ 100 km), closing a sub-THz link becomes challenging due to the large spreading, absorption, and scattering losses. Recent advancements, as outlined in Section 2, have made closing the link at sub-THz frequencies possible.

In Table 1, we outline link parameters derived from the reviewed state-of-the-art hardware. Based on absorption windows and available FCC licensing discussed in Section 1, a carrier frequency of 225 GHz (for downlink communications) is chosen. Physical parameters are chosen to match the state-of-the-art, assuming a 45 dBi satellite antenna gain and 65 dBi ground station antenna gain. Additionally, an output power of 315 mW (25 dBm) was used as an estimate for a flight-qualified analog front-end. Along with spreading loss, the presented analysis ac-

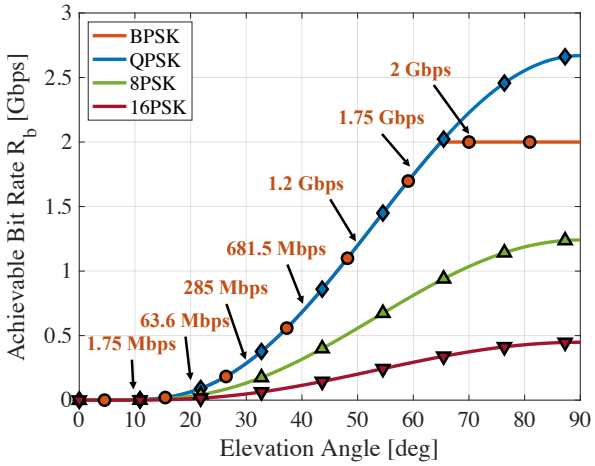

(a) Bit rate as a function of ground station elevation angle

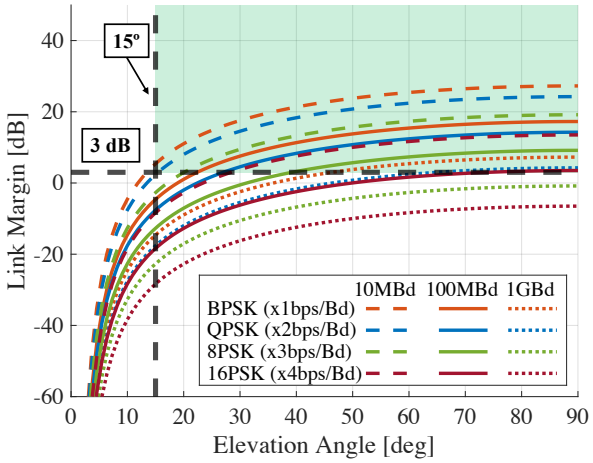

(b) Link margin as a function of ground station elevation angle

Figure 1: Link analysis with state-of-the-art sub-THz hardware

counts for molecular absorption loss, L_{abs}, computed as follows:

$$L_{\text{abs}}(f_c, d(e)) = \exp\left[\int_0^{d(e)} \kappa(f_c, Q(r), p(r), T(r))dr\right], \quad (2)$$

where f_c is the carrier frequency, $d(e)$ is the distance between the satellite and the ground site, which varies for different elevation angles e, and κ is the molecular absorption coefficient for the atmosphere, which depends on the composition $Q(r)$, the pressure $p(r)$, and the temperature $T(r)$ profiles. These parameters, in turn, change along the propagation path and elevation angle. These profiles, along with the dependence of κ on them, are obtained from the ITU Recommendation ITU-R P.676-12[60] as well as Recommendation ITU-R P.835.[61]

The analysis models an orbit at 416 km altitude. In line with common satellite link budget practices, a safety margin of 3 dB is considered for link closure. Other parameters include a 0.3 roll-off factor for the Square-Root Raised Cosine (SRRC) pulse, as well as a target Bit Error Rate (BER) of 10^{-4}.

Results are reported in Figure 1. In Figure 1a, we determine the achievable bit rate for various modulation orders at varying elevation angles, while, in Figure 1b, we show the link margin for varying elevation angles at multiple combinations of symbol rate and modulation order. Notably, only phase modulations are considered due to their constant signal envelope. That is, to maximize the output power of sub-THz front ends, all the amplifiers operate close to their saturation point. Thus, small variations in the amplitude of the input signals result in an inadequate response of the amplifiers, resulting in less output power. To avoid this, the input signals should have a constant amplitude or envelope.

Table 1: Link budget parameters for state-of-the-art sub-THz hardware

Parameter	Value
State-of-the-art sub-THz hardware	
Carrier Frequency	225 GHz
Maximum Symbol Rate	2 GBd
Transmit Power	25 dBm (315 mW)
CubeSat Antenna Gain	45 dBi
Ground Station Antenna Gain	65 dBi
Receiver Noise Figure	7 dB
Additional Parameters	
Orbital Altitude	416 km
Link Margin	3 dB
Roll-off Factor	0.3
Target BER	10^{-4}

From Figure 1a, we observe that, while the achievable bit rate is heavily dependent on elevation angle, as expected, the maximization of the bit rate, thanks to large Signal-to-Noise Ratio (SNR), is possible (for BPSK and at elevation angles past 65°). Furthermore, the power limitation of sub-THz sources results in the highest bit rates only achievable through the lowest modulation orders. Specifically, 100 Mbps transmissions are achievable past 25°, with even higher bit rates of over 1 Gbps achievable past 47°, only with BPSK and QPSK. While sub-THz link performance is largely dependent on

elevation angle–and thus by the specific ground station pass experienced–high bit rates (> 100 Mbps) can still be achieved even at relatively low elevation angles.

In Figure 1b we find similar trends. The green shaded region identifies the region in which a link can be considered closed, i.e. elevation angles above 15° and link margins > 3 dB. Curves representing different combinations of modulation orders and symbol rates enter this region at different elevation angles. Directly at 15°, the link closes for the lowest symbol rate considered (10 MBd) with BPSK and QPSK. By 30°, multiple combinations of symbol rate and modulation order are capable of closing the link, including both BPSK and QPSK at a 100 MBd. Higher symbol rates and modulation orders require much higher data rates to close the link, with some combinations unable to cross the 3 dB margin. Nonetheless, through Figure 1 we determine that the sub-THz link can close at low elevation angles and achieve high bit rates even with the lowest modulation orders.

4 SUB-THZ PAYLOAD DESIGN AND PERFORMANCE RESULTS

After the evaluation of the state-of-the-art hardware and the observations drawn from the link budget analysis, we conclude that sub-THz communication is ready for space. In this section, we propose the first design of a sub-THz transceiver that showcases the necessary characteristics to realize this opportunity. While it is not the focus of the present manuscript, we note that the proposed design is part of Northeastern University's TeraLink CubeSat mission, which will utilize this payload to close a sub-THz satellite UL and DL for the first time.

As such, specific design choices and payload operations discussed follow the requirements necessary to achieve mission success, as defined by TeraLink's mission success criteria. Key mission factors influencing the radio design include the satellite not performing direct decoding of sub-THz signals, but rather capturing raw I/Q samples through a separate telemetry, tracking and control (TT&C) link, as well as aligning SWaP considerations for a 6U form factor. Additionally, the payload will be expected to operate at symbol rates and modulation orders outlined in Table 2, in line with the showcased link analysis. Aside from these specifics, the proposed design aims to showcase the potential for implementing sub-THz communication payloads in space-based applications beyond this mission.

Table 2: Payload symbol rates and modulation orders

Modulations	Symbol Rates (R_s)
BPSK	10 MBd
QPSK	100 MBd
8-PSK	1 GBd
16-PSK	

Antenna Design

Based on the trade-offs discussed in Section 2, the horn antenna array is selected as the most suitable solution for spacecraft integration. In particular, we constrain the design to fit within a 1U CubeSat footprint, minimize weight, and achieve a target gain of approximately 45 dBi. Key design considerations include physical size, weight, gain, efficiency, and fabrication cost.

In this section, we present the horn array configuration, describe its structure, and provide electromagnetic simulation results obtained using Altair Feko to demonstrate its potential to achieve high gain with the constraints of a CubeSat platform.

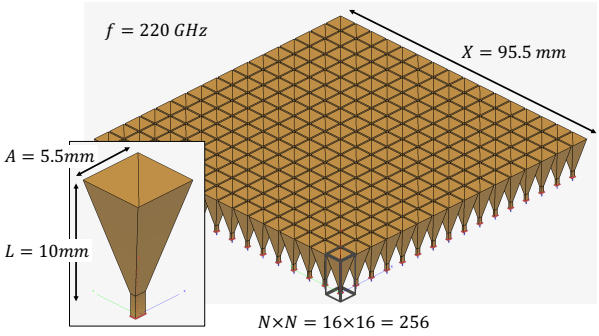

Figure 2: Horn antenna array

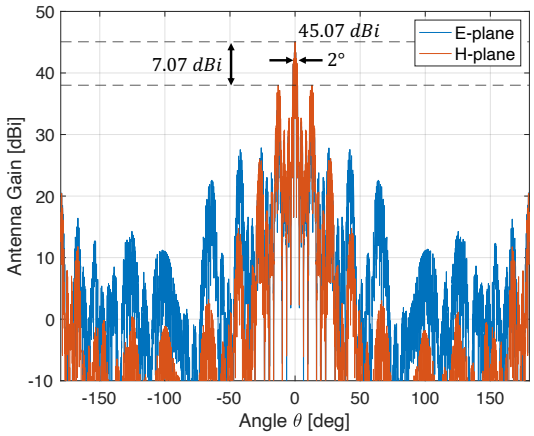

Figure 3: Simulated radiation pattern of a 16×16 horn antenna array at 220 GHz.

Since individual horn antennas already provide high directivity, fewer elements are needed to reach target gains when arraying them. Specifically, we propose a 220 GHz horn design with a length of $L = 10$ mm and a flare width of $A = 5.5$ mm, which achieves a gain of 21 dBi. A 16×16 array of these horns is then arranged within the 10 cm×10 cm frontal aperture of a 1U CubeSat, thus resulting in a theoretical array factor gain of 24.08 dB, and, thus, a total gain of 45.08 dBi.

We validate this using Altair Feko. The 16×16 array, shown in Figure 2, is confirmed to achieve a peak gain of 45.07 dBi. The spacing between each horn is set to $s = 6$ mm. The corresponding E-plane and H-plane radiation pattern results are shown in Figure 3. From the plot, a side-lobe level of 7.07 dB is observed, with secondary lobes appearing at an angle of 13° from broadside. The 3 dB beamwidth is 2°. It is worth noting that, in practice, some performance degradation is expected due to fabrication tolerances and conduction losses.

While these results showcase high gain, efficient use of aperture, and compact integration, the main design challenge lies in the feeding network of the horns, which must ensure equal amplitude and phase at each element. This can be implemented using power dividers or multiple synchronized sources. Despite this added complexity, the horn array requires less intricate feed design and fabrication compared to arrays based on quasi-omnidirectional elements such as patch antennas. In those cases, a significantly larger number of elements would be needed to achieve comparable gain, and the element dimensions become comparable to the wavelength, further complicating the design and integration.

Additionally, horn antenna arrays are well-suited for fabrication using conventional CNC machining, which provides the necessary dimensional precision and surface finish at sub-THz frequencies. With tolerances on the order of tens of micrometers and minimum feature sizes in the few hundred micrometer range, CNC machining can reliably produce the ∼0.5 mm waveguide apertures required in this design—these being the most critical dimensional constraints. This makes CNC a practical and cost-effective alternative to more advanced micromachining techniques.

Analog Front End Design

In Figure 4, we report the preliminary design for the analog front-end of the proposed payload. Operating at 210-240 GHz, this design utilizes Schottky-diode frequency multipliers to upconvert a shared variable local oscillator (VLO) signal ranging from 24-26 GHz. Modulation occurs through an in-phase and quadrature (IQ) mixer fed by both the encoded baseband signal from the RFSoC and the variable oscillator output. The resulting modulated intermediate carrier is then upconverted by a factor of three and filtered prior to feeding the Tx antenna. In reception, the signal is downconverted through an IQ demodulator fed by the multiplied output of the local oscillator at sub-THz frequencies. This splits the received signal into separate I and Q streams, which are fed into the RFSoC for baseband processing. Two separate carrier frequencies are chosen for transmitting and receiving in line with current FCC regulations in this sub-THz band.[32]

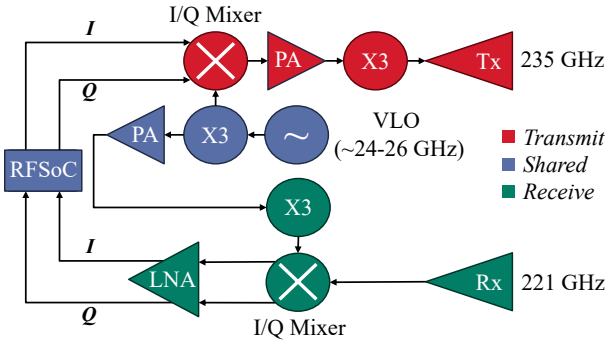

Figure 4: Preliminary sub-THz analog front-end block diagram

Direct up/down conversion, i.e. IQ analog mixing, was chosen for its ability to boost overall system bandwidth and enhance post-processing capabilities. Mixing through Intermediate Frequency (IF) architectures requires the digital modulation of an IF carrier, thus generating a sideband image of the transmitted signal, and reducing the usable bandwidth of the RFSoC's data converters by 50 %. Conversely, modulating the carrier directly from digital baseband, IQ mixing inherently avoids these spectral images and enables greater utilization sampling rate of the data converters. Furthermore, conversion losses are hence reduced in IQ mixing as less signal power is wasted on undesired images, thus improving overall power efficiency.

Digital Signal Processing Engine

The DSP engine selected for both data conversion (analog-to-digital and digital-to-analog) and subsequent signal processing tasks is an RFSoC. As indicated in Section 2, RFSoCs provide high-speed data conversion capabilities, reducing reliance on external RF front end components, while meeting the required speed and achieving the necessary SWaP efficiency.

Figure 5 illustrates the proposed baseband sig-

nal processing design and its key functionalities. As discussed, data conversion is performed directly at baseband to maximize the usable bandwidth within the first Nyquist zone of the converters, as employing IF digital upconversion would reduce the usable bandwidth by half. As shown, the current sampling rate (f_s) configuration enables at least four samples per symbol (SPS) at symbol rates (R_s) of up to 1 GBd, providing sufficient resolution for high-fidelity digital modulation schemes (SPS $= f_s/R_s$).

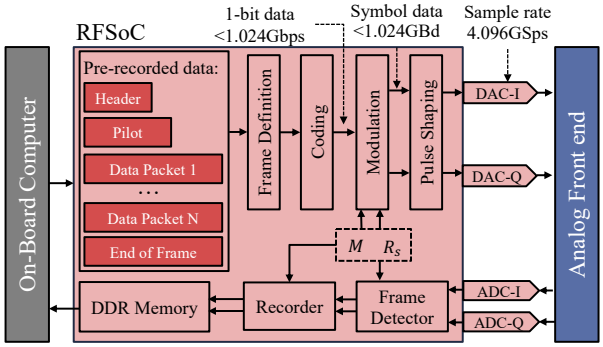

Figure 5: Overview of the high-speed digital signal processing engine.

As indicated in the figure, the RFSoC is the component of the payload that interfaces directly with the On Board Computer (OBC). Communication between the two is established via a TCP connection over Ethernet using an RJ-45 connector. In the forward direction, the OBC is programmed to control the RFSoC by issuing commands to power it on or off, configure the upcoming experiment parameters, and initiate or terminate transmission or reception. The experiment configuration includes parameters such as symbol rate, modulation scheme, and coding strategy, as defined by the design requirements outlined in Section 3. In the reverse direction, the OBC retrieves the stored IQ samples resulting from an uplink experiment.

Inside the RFSoC, the following functions are performed in transmission:

- **Frame Definition**: The process of structuring data into a well-defined format before transmission. It selects the corresponding data packet to be transmitted and appends the rest of the frame fields (Header, Pilot, and end of frame (EOF)) before the next block.
- **Coding**: Encodes the transmitted bits by adding redundant information that will help the receiver decrease the probability of an error in a demodulated bit. Currently, linear block codes like Polar Codes or Low-Density Parity Check Codes are utilized due to their efficient implementation in transmission (matrix multiplication).
- **Modulation**: This block converts digital data (bits) into a waveform suitable for transmission by the phase of the carrier signal. The resulting outputs are complex values representing the amplitude and the phase of the signal to be transmitted. These complex numbers are sent to the Analog Front End by separating the real and imaginary parts as the In-phase ($I[n]$) and Quadrature ($Q[n]$) components of the signal, respectively.
- **Pulse Shaping**: Smooths the transmitted signal to improve spectral efficiency, ensuring the signal minimizes its used bandwidth without excessive distortion. This greatly enhances the SNR at the receiver, as the bandwidth of the filter used in reception is greatly reduced, thus minimizing in-band noise. A SRRC pulse with a roll-off factor $\alpha = 0.3$ is utilized.

Conversely, since the resulting data product from an experiment of the TeraLink mission is directly the IQ samples of the received signal, the architecture of the receiver is much simpler, consisting of a Frame Detector, a Recorder block, and the Double Data Rate (DDR) memory:

- **Frame Detector**: In charge of detecting the incoming frames and enabling recording only when packets are detected, thus utilizing memory efficiently.
- **Recorder**: Performs sample averaging when possible, and records the captured samples in the DDR memory of the board. The recording time is configured according to the modulation order, symbol rate, and coding rate of the transmission, as these parameters uniquely define the duration of the transmission.
- **DDR Memory**: Stores the received IQ samples to be read from the OBC.

The proposed radio is designed to transmit a single type of frame, focusing on simplicity and robustness. Concretely, the transmitted frames will have the following fields:

- **Header Preamble (128 bits)**: The header is a short sequence at the beginning of each transmission that allows the receiver to recognize the start of a valid data frame. It ensures synchronization so the data is processed correctly.
- **Pilot Sequence (256 bits)**: The pilot sequence consists of known reference signals embedded in the transmission. These signals allow the receiver to measure and correct for any distortions caused by the space environment or

communication channel, improving data accuracy. Golay sequences will be utilized for this purpose.

- **Data (1024 bits)**: This is the main content of the transmission, which is utilized to compute BER measurements and assess the correct or incorrect demodulation of the transmitted information. The content of this field consists of pre-recorded data on board the RFSoC, currently consisting of a low-resolution JPEG image.
- **EOF Preamble (32 bits)**: A predefined sequence marking the end of a transmission. It ensures the receiver correctly identifies where the data frame finishes, preventing partial or misinterpreted messages.

The total length of the frame is, thus, 1440 bits. Assuming the transmission of an image occupying 236kB (mid-low resolution JPEG image), we derive the expected data to be generated per transmission. With 1024 bits of image data per frame, a total of 1844 frames are expected per transmission. The maximum amount of data generated will occur with the slowest transmission symbol rate ($R_s = 8MBd$) and modulation order ($M = 2$), as the transmission will take more time and, correspondingly, more samples will need to be acquired and stored. Assuming the sampling rate of 4.096 GSps, a sampling resolution of 14 bit/sample, a sampling time margin of 50%, and a sample averaging factor of 128, the maximum amount of data generated will be 55.92 MB.

The specific RFSoC selected for the proposed design is the third-generation AMD Zynq UltraScale+ RFSoC, specifically the ZU48DR. This device supports 14-bit DACs operating at up to 10 GSps and ADCs at up to 5 GSps. These sampling speeds allow for signal bandwidths of more than 1 GHz while satisfying the Nyquist theorem, thus allowing for the implementation of the data-rates outlined in Fig. 1. The chosen carrier board is the HTG-ZRF8 from HiTech Global, which integrates the data converter interfaces directly on the main board, eliminating the need for external daughter cards. This integration results in a compact footprint of just 11×17 cm^2, significantly enhancing the overall compactness of the payload. Current power consumption estimates fall between 5 and 10 W.

Performance Analysis

An important factor to consider for any satellite hardware is power consumption. In the space environment, available power is highly restricted and must be carefully allocated to all onboard systems. These constraints arise from factors such as orbit, duty cycle of the experiment, satellite size, and efficiency of power generation among others. Table 3 summarizes a preliminary power analysis for the proposed sub-THz payload from estimates of the state-of-the-art.

Table 3: Preliminary power analysis of state-of-the-art sub-THz hardware

Component	Power Draw
Analog Front End	
Power Amplifiers	2 x 5 W
x3 Multiplier	2 x 0.2 W
Local Oscillator	8 W
Mixer	0 W
Low Noise Amplifier	< 0.2 W
Digital Signal Processing	
RFSoC	5-10 W
Total Power	**23.6-28.6 W**
75% DC-DC Efficiency	**31.5-38.1 W**

Despite the relatively high power draw for this payload, these values are well within the consumption of similar high data-rate-seeking missions. At the current state-of-the-art for FSO payloads, power consumption for terminals range from around 10 W to as high as 100 W, with a median value of 23 W.[62] Achieving lower data rates, commercial satellite communication systems operating in X-band and Ka-band have power draws that fall within similar ranges.[63–65] Although the power draw for this sub-THz payload requires mission design to ensure that a satellite can support its operation, this design is not uncommon given the state-of-the-art for other high data-rate communications systems for space.

In addition to power draw, an essential parameter for the payload is RF output power. Before flight, it is necessary to validate link budgets through experimental analysis of the satellite performance. As such, the TeraNova testbed platform[66] was used to evaluate the output for a 225 GHz transmitter built by NASA JPL, utilized for previous multi-kilometer tests,[50] and a candidate engineering model considered for the flight design discussed earlier in this section. Measurements were taken utilizing the VDI PM5B power meter connected directly to the output of the transmitter, with the conversion losses of the equipment factored into the results. A sweep of the local oscillator frequency was carried out in steps of 2 GHz for different bias voltages to the final multiplier to observe the output power through the full frequency range of the front ends.

The results, reported in Figure 6, indicate that current engineering models for the proposed fre-

quency bands can reach high output power levels required for long link distances. Additionally, these front ends were developed over 5 years ago, and as indicated in Section 2, recent advancements in sub-THz analog technology have pushed output power beyond these measurements. For a finalized flight model with the current available hardware, output power levels can push well beyond these results into the range of 315 mW (25 dBm).

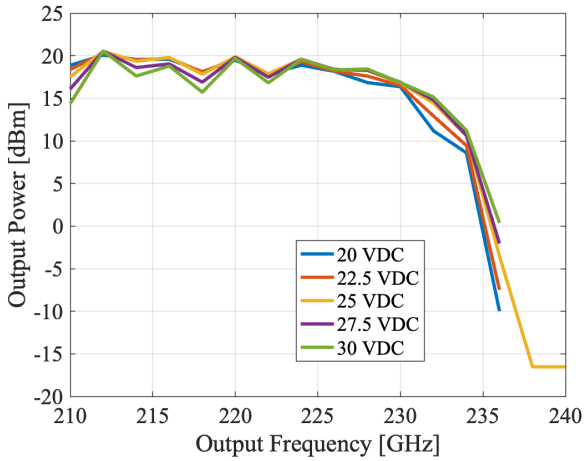

Figure 6: Output power sweep for 210-240 GHz JPL front-ends at different bias values in the final tripler

Volume Analysis

Regardless of the type of mission, whether small satellite or much larger spacecraft, volume is an essential factor to consider if a system is space-ready. For communications, hardware must coexist with not only the satellite's vital avionics and payload but also other systems that might be used for individual purposes (beacons, telemetry, control, etc.).

Up until recently, an end-to-end sub-THz system was not compatible with a satellite form factor due to bulky AWGs and DSOs required, as well as inefficiently packaged engineering model front ends designed for in-lab testing. The advancement of terahertz hardware, mainly the advent of compact RFSoCs and commercially available sub-THz front ends, has greatly reduced the footprint that these systems occupy.

By selecting candidate hardware from the state-of-the-art, a preliminary volume analysis is established. Beginning with the antennas, two identical horn antenna arrays (one for transmitting chain and one for receiving) can be used with each (if considering a 16×16 array) estimated to occupy around 9 cm $\times$ 9 cm surface area with a 2 cm thickness. Next, a current engineering unit for the analog front ends, as utilized for results in Section 4, occupies 17 cm $\times$ 8 cm $\times$ 9 cm for transmitting, and 14 cm $\times$ 7 cm $\times$ 7 cm for receiving. Finally, third-generation AMD Zynq UltraScale+ RFSoC, as discussed in Section 4, will occupy around 11×17 cm^2. This reaches a total upper bound in volume of around 3.6U, as this does not consider further efficient packaging and design that will be used for the flight unit.

In comparison with similar high-frequency communications systems like optical terminals or Ka-band radios, this volume estimate is comparable with other novel communications-focused missions like NASA's TBIRD optical payload, which occupied a 3U volume on a 6U CubeSat.[67] Notably, this payload will be the first of its kind, meaning further iterations and improvements to a potential commercial off-the-shelf (COTS) model for a sub-THz communication system may reduce this volume.

5 CONCLUSIONS AND NEXT STEPS

In this paper, the first design of a sub-THz radio for satellite communications is presented. Along with a review of the state-of-the-art sub-THz technology, including antennas, analog front-ends, and DSP engines, we show that sub-THz communications is nearing readiness for space-flight. Selected hardware parameters are confirmed to close a link from/to LEO with bit rates exceeding 100 Mbps. Additionally, power and volume estimates are analyzed and found to be comparable to much lower data rate communications payloads using alternative technologies in the optical and RF bands. Finally, block diagrams for individual components of the payload, as well as hardware characterization results, are presented, proving that flight-ready sub-THz hardware is just around the corner.

Immediate next steps include end-to-end integration and verification of the proposed design, followed by experimental validation. For this purpose, a functional prototype will be implemented with existing non-flight-qualified hardware, while the flight-qualified version will be designed in parallel based on the obtained learnings. The flight radio will be assembled in an adequately rated clean-room environment and integrated with Northeastern University's TeraLink CubeSat mission, which is slated to launch in 2027 through NASA's CubeSat Launch Initiative (CSLI)[68] (referred to as THIS-SAT).

The successful deployment and in-orbit verification of the proposed sub-THz radio will mark a new era in satellite communications by unlocking underutilized spectrum and alleviating congestion in the overcrowded RF bands. While future iterations will

focus on increasing the Technology Readiness Level (TRL), dedicated designs for ISLs will require targeted adaptations. Ultimately, the validation of sub-THz and THz high-data-rate payloads in space is poised to redefine satellite networks and constellations, paving the way for advanced research in areas such as estimation and equalization of the (sub-)THz satellite channel, MAC protocol optimization, and space Internet routing, to name some.

References

1. John Venable. US Space Force. *The Heritage Foundation*, 2021.

2. David J Weeks, Steven H Walker, and Robert L Sackheim. Small satellites and the DARPA/Air Force FALCON program. *Acta Astronautica*, 57(2-8):469–477, 2005.

3. Nils Pachler, Inigo del Portillo, Edward F. Crawley, and Bruce G. Cameron. An Updated Comparison of Four Low Earth Orbit Satellite Constellation Systems to Provide Global Broadband. In *Proc. of the IEEE ICC Workshops*, pages 1–7, June 2021.

4. Marshall Smith, Douglas Craig, Nicole Herrmann, Erin Mahoney, Jonathan Krezel, Nate McIntyre, and Kandyce Goodliff. The Artemis Program: An Overview of NASA's Activities to Return Humans to the Moon. In *2020 IEEE Aerospace Conference*, pages 1–10, 2020.

5. Kenneth A. Farley, Kenneth H. Williford, Kathryn M. Stack, Rohit Bhartia, Al Chen, Manuel de la Torre, Kevin Hand, Yulia Goreva, Christopher D. K. Herd, Ricardo Hueso, Yang Liu, Justin N. Maki, German Martinez, Robert C. Moeller, Adam Nelessen, Claire E. Newman, Daniel Nunes, Adrian Ponce, Nicole Spanovich, Peter A. Willis, Luther W. Beegle, James F. Bell, Adrian J. Brown, Svein-Erik Hamran, Joel A. Hurowitz, Sylvestre Maurice, David A. Paige, Jose A. Rodriguez-Manfredi, Mitch Schulte, and Roger C. Wiens. Mars 2020 Mission Overview. *Space Science Reviews*, 216(8):142, December 2020.

6. NASA Strategic Plan 2022, 2022. Accessed: January 2024.

7. Claudio Corti, Kathryn Whitman, Ravindra Desai, Jamie S. Rankin, Du Toit Strauss, Nariaki Nitta, Drew Turner, and Thomas Y. Chen. Galactic Cosmic Rays and Solar Energetic Particles in Cis-Lunar Space. *Bulletin of the AAS*, July 2023.

8. Steve Creech, John Guidi, and Darcy Elburn. Artemis: An Overview of NASA's Activities to Return Humans to the Moon. In *2022 IEEE Aerospace Conference (AERO)*, pages 1–7, March 2022.

9. Ricardo Arevalo Jr, Ziqin Ni, and Ryan M. Danell. Mass spectrometry and planetary exploration: A brief review and future projection. *Journal of Mass Spectrometry*, 55(1):e4454, 2020.

10. Meesha Sundarum. Update on 5G Non-Terrestrial Networks Briefing Paper, July 2023.

11. New Speedtest Data Shows Starlink Users Love Their Provider, May 2023.

12. Edwin Goh, Hamsa Shwetha Venkataram, Mark Hoffmann, Mark D. Johnston, and Brian Wilson. Scheduling the NASA Deep Space Network with Deep Reinforcement Learning. In *2021 IEEE Aerospace Conference (50100)*, pages 1–10, 2021.

13. Lee, Carlyn-Ann, Andrew Kwok, Kristy Tran, Janet P. Wu, Yijiang Chen, David P. Heckman, Bruce E. MacNeal, and Douglas S. Abraham. Recommendations Emerging from an Analysis of NASA's Deep Space Communications Capacity. Pasadena, CA: Jet Propulsion Laboratory, National Aeronautics and Space Administration, 2018. Document ID: 20210008288.

14. Michael Dumiak. SpaceX and Dish's Super-Shady War for the World - IEEE Spectrum, July 2022.

15. Michele Polese, Xavier Cantos-Roman, Arjun Singh, Michael J. Marcus, Thomas J. Maccarone, Tommaso Melodia, and Josep Miquel Jornet. Coexistence and Spectrum Sharing Above 100 GHz. *Proceedings of the IEEE*, 111(8):928–954, 2023.

16. Giacomo Curzi, Dario Modenini, and Paolo Tortora. Large Constellations of Small Satellites: A Survey of Near Future Challenges and Missions. *Aerospace*, 7(99):133, September 2020.

17. Oltjon Kodheli, Eva Lagunas, Nicola Maturo, Shree Krishna Sharma, Bhavani Shankar, Jesus Fabian Mendoza Montoya, Juan Carlos Merlano Duncan, Danilo Spano, Symeon Chatzinotas, Steven Kisseleff, Jorge Querol, Lei Lei, Thang X. Vu, and George Goussetis. Satellite

Communications in the New Space Era: A Survey and Future Challenges. *IEEE Communications Surveys & Tutorials*, 23(1):70–109, 2021.

18. Curt M. Schieler, Kathleen M. Riesing, Bryan C. Bilyeu, Bryan S. Robinson, Jade P. Wang, W. Tom Roberts, and Sabino Piazzolla. TBIRD 200-Gbps CubeSat Downlink: System Architecture and Mission Plan. In *2022 IEEE International Conference on Space Optical Systems and Applications (ICSOS)*, pages 181–185, March 2022.

19. Kerri Cahoy, Peter Grenfell, Angela Crews, Michael Long, Paul Serra, Anh Nguyen, Riley Fitzgerald, Christian Haughwout, Rodrigo Diez, Alexa Aguilar, John Conklin, Cadence Payne, Joseph Kusters, Chloe Sackier, Mia LaRocca, and Laura Yenchesky. The CubeSat Laser Infrared CrosslinK Mission (CLICK). In *International Conference on Space Optics — ICSO 2018*, volume 11180, pages 358–369. SPIE, July 2019.

20. Hemani Kaushal and Georges Kaddoum. Optical Communication in Space: Challenges and Mitigation Techniques. *IEEE Communications Surveys & Tutorials*, 19(1):57–96, 2017.

21. M. Dresscher, C. W. Korevaar, N. C. J. van der Valk, T. J. de Lange, R. Saathof, N. Doelman, W. E. Crowcombe, C. M. Duque, H. de Man, J. D. Human, G. Witvoet, N. van der Heiden, R. den Breeje, S. Kuiper, and E. C. Fritz. Key Challenges and Results in the Design of Cubesat Laser Terminals, Optical Heads and Coarse Pointing Assemblies. In *2019 IEEE International Conference on Space Optical Systems and Applications (ICSOS)*, pages 1–6, October 2019.

22. Yunus Emre Kahraman and Ahmet Akbulut. Investigation of the Effects of Pointing Errors on Optical Intersatellite Links Using Real Orbital Data. In *2021 8th International Conference on Electrical and Electronics Engineering (ICEEE)*, pages 273–276, April 2021.

23. Larry C. Andrews and Ronald L. Phillips. *Laser beam propagation through random media*. SPIE Press, Bellingham, Wash, 2nd ed edition, 2005.

24. Daniel A. Goldman, Paul Serra, Shreeyam Kacker, Lucas Benney, Daniel Vresilovic, Steven J. Spector, Kerri Cahoy, and Jordan S. Wachs. MOEMS-Based Lens-Assisted Beam Steering for Free-Space Optical Communications. *Journal of Lightwave Technology*, 41(9):2675–2690, May 2023.

25. Benjamin Rödiger, Rene Rüddenklau, Christopher Schmidt, and Marc Lehmann. Acquisition Concept for Inter-Satellite Communication Terminals on CubeSats. In *Small Satellites Systems and Services - The 4S Symposium 2022*, Vilamoura, Portugal, May 2022.

26. Hannah Tomio, Peter Grenfell, William Kammerer, Paul Serra, Ondrej Čierny, Charles Lindsay, Maddie Garcia, Kerri Cahoy, Myles Clark, Danielle Coogan, John Conklin, David Mayer, Jan Stupl, and John Hanson. Development and Testing of the Laser Transmitter and Pointing, Acquisition, and Tracking System for the CubeSat Laser Infrared CrosslinK (CLICK) B/C Mission. In *2022 IEEE International Conference on Space Optical Systems and Applications (ICSOS)*, pages 224–231, March 2022.

27. Nasir Saeed, Ahmed Elzanaty, Heba Almorad, Hayssam Dahrouj, Tareq Y. Al-Naffouri, and Mohamed-Slim Alouini. CubeSat Communications: Recent Advances and Future Challenges. *IEEE Communications Surveys & Tutorials*, 22(3):1839–1862, 2020.

28. Marco Giordani and Michele Zorzi. Non-Terrestrial Networks in the 6G Era: Challenges and Opportunities. *IEEE Network*, 35(2):244–251, April 2021.

29. Akhtar Saeed, HE Yaldiz, and Fatih Alagoz. GHz-to-THz broadband communications for 6G non-terrestrial networks. *ITU Journal on Future and Evolving Technologies*, 4(1):241–250, 2023.

30. A. Masihi, P. Testolina, and Josep M. Jornet. Terahertz vs. Optical for Inter-Satellite Links: A Comparative Analysis of Pointing Errors and System Performance. In *Proc. of the 2nd Workshop on Emerging Technologies in Aerial and Space Networks, in conjunction with IEEE ICC 2025*, Montreal, Canada, June 8–12 2025. to appear.

31. Chong Han, Weijun Gao, Nan Yang, and Josep M Jornet. Molecular Absorption Effect: A Double-edged Sword of Terahertz Communications. *IEEE Wireless Communications*, 2022.

32. Federal Communications Commission. FCC Table of Frequency Allocations, 2025. Accessed: 2025-05-30.

33. Priyangshu Sen, Viduneth Ariyarathna, Arjuna Madanayake, and Josep M. Jornet. A versatile experimental testbed for ultrabroadband communication networks above 100 GHz. *Computer Networks*, 193:108092, July 2021.

34. I. F. Akyildiz, C. Han, Z. Hu, S. Nie, and J. M. Jornet. Terahertz band communication: An old problem revisited and research directions for the next decade. *IEEE Transactions on Communications*, 70(6):4250–4285, 2022.

35. Suhila Abulgasem, Faisel Tubbal, Raad Raad, Panagiotis Ioannis Theoharis, Sining Lu, and Saeid Iranmanesh. Antenna Designs for CubeSats: A Review. *IEEE Access*, 9:45289–45324, 2021.

36. Yahya Rahmat-Samii and Arthur C. Densmore. Technology Trends and Challenges of Antennas for Satellite Communication Systems. *IEEE Transactions on Antennas and Propagation*, 63(4):1191–1204, April 2015.

37. Zhao Wu, Long Li, Yongjiu Li, and Xi Chen. Metasurface Superstrate Antenna With Wideband Circular Polarization for Satellite Communication Application. *IEEE Antennas and Wireless Propagation Letters*, 15:374–377, 2016.

38. Kimmo Rasilainen, Tung Duy Phan, Markus Berg, Aarno Pärssinen, and Ping Jack Soh. Hardware Aspects of Sub-THz Antennas and Reconfigurable Intelligent Surfaces for 6G Communications. *IEEE Journal on Selected Areas in Communications*, 41(8):2530–2546, August 2023.

39. Feng Xie, Zhang-Cheng Hao, Zekun Li, Jia-Ying Zhang, Zi-Jun Guo, Chen-Yu Ding, Zhuo-Wei Miao, Jixin Chen, Zhengbo Jiang, and Wei Hong. A 220-GHz Planar Triangular Lattice Transmitter Array With 42.7-dBm Peak EIRP for Long-Distance High-Data-Rate Wireless Communication. *IEEE Transactions on Microwave Theory and Techniques*, pages 1–15, 2024.

40. S.S. Gill, Hemant Arora, Jidesh, and Viren Sheth. On the development of Antenna feed array for space applications by additive manufacturing technique. *Additive Manufacturing*, 17:39–46, October 2017.

41. Xibi Chen, Nathan M. Monroe, Georgios C. Dogiamis, Robert A. Stingel, Preston Myers, and Ruonan Han. A 265-GHz CMOS Reflectarray With 98×98 Elements for 1°-Wide Beam Forming and High-Angular-Resolution Radar Imaging. *IEEE Journal of Solid-State Circuits*, 59(11):3655–3669, November 2024.

42. Josep M Jornet, Vitaly Petrov, Hua Wang, Zoya Popović, Dipankar Shakya, Jose V Siles, and Theodore S Rappaport. The evolution of applications, hardware design, and channel modeling for terahertz (THz) band communications and sensing: Ready for 6G? *Proceedings of the IEEE*, 2024.

43. Bilal Barut, Xavier Cantos-Roman, Justin Crabb, Chun-Pui Kwan, Ripudaman Dixit, Nargess Arabchigavkani, Shenchu Yin, Jubin Nathawat, Keke He, Michael D. Randle, Farah Vandrevala, Takeyoshi Sugaya, Erik Einarsson, Josep M. Jornet, Jonathan P. Bird, and Gregory R. Aizin. Asymmetrically Engineered Nanoscale Transistors for On-Demand Sourcing of Terahertz Plasmons. 22(7):2674–2681, 2022. Published: March 21, 2022.

44. A. N. Grigorenko, M. Polini, and K. S. Novoselov. Graphene plasmonics. 6(11):749–758, 2012.

45. Benjamin S. Williams. Terahertz quantum-cascade lasers. *Nature Photonics*, 1:517–525, 2007.

46. Alessia Sorgi, Marco Meucci, Muhammad A. Umair, Francesco Cappelli, Guido Toci, Paolo De Natale, Leonardo Viti, Andrea C. Ferrari, Miriam S. Vitiello, Luigi Consolino, and Jacopo Catani. QCL-Based Cryogen-Free THz Optical Wireless Communication Link. *Laser & Photonics Reviews*, 18(1):202301082, 2024.

47. Andreas Stohr and Dieter Jdger. Photonic Millimeter-wave and Terahertz Source Technologies (invited paper). In *2006 International Topical Meeting on Microwave Photonics*, pages 1–4, 2006.

48. Ullrich R. Pfeiffer, Chinmaya Mishra, Robert M. Rassel, Shawn Pinkett, and Scott K. Reynolds. Schottky Barrier Diode Circuits in Silicon for Future Millimeter-Wave and Terahertz Applications. *IEEE Transactions on Microwave Theory and Techniques*, 56(2):364–371, 2008.

49. Imran Mehdi, Jose Siles, Christine P. Chen, and Josep M. Jornet. THz Technology for Space Communications. In *2018 Asia-Pacific Microwave Conference (APMC)*, pages 76–78, 2018.

50. Priyangshu Sen, Jose V Siles, Ngwe Thawdar, and Josep M Jornet. Multi-kilometre and multi-gigabit-per-second sub-terahertz communications for wireless backhaul applications. *Nature Electronics*, 6(2):164–175, 2023.

51. Yinian Feng, Bo Zhang, Chen Zhi, Ke Liu, Weilong Liu, Fang Shen, Chuanqi Qiao, Jicong Zhang, Yong Fan, and Xiaobo Yang. A 20.8-Gbps dual-carrier wireless communication link in 220-GHz band. *China Communications*, 18(5):210–220, 2021.

52. J. Zhang *et al.* 6G Oriented 100 GbE Real-time Demonstration of Fiber-THz-fiber Seamless Communication Enabled by Photonics. In *Proc. of OFC Demo Zone*, 2022.

53. Shi Jia, Mu-Chieh Lo, Lu Zhang, Oskars Ozolins, Aleksejs Udalcovs, Deming Kong, Xiaodan Pang, Robinson Guzman, Xianbin Yu, Shilin Xiao, et al. Integrated dual-laser photonic chip for high-purity carrier generation enabling ultrafast terahertz wireless communications. *Nature Communications*, 13(1):1–8, 2022.

54. Huawei Technologies. 6G ISAC-THz Opens up New Possibilities for Wireless Communication Systems, 2022.

55. National Instruments. Creating a Sub-Terahertz Testbed with the NI mmWave Transceiver System. White Paper, September 2019.

56. Keysight Technologies. A New Sub-Terahertz Testbed for 6G Research. White Paper, 2020.

57. Hussam Abdellatif, Viduneth Ariyarathna, Arjuna Madanayake, and Josep Miquel Jornet. A Real-Time Software-Defined Radio Platform for Sub-Terahertz Communication Systems. *IEEE Access*, 12:146315–146327, 2024.

58. National Instruments. Introduction to the NI mmWave Transceiver System Hardware, n.d.

59. Shadi Abu-Surra, Wonsuk Choi, Sungtae Choi, Eunyoung Seok, Dongjoo Kim, Navneet Sharma, Siddharth Advani, Vitali Loseu, Kitaek Bae, Ilju Na, Ali A. Farid, Mark J. W. Rodwell, Gary Xu, and Jianzhong Charlie Zhang. End-to-end 140 GHz Wireless Link Demonstration with Fully-Digital Beamformed System. In *2021 IEEE International Conference on Communications Workshops (ICC Workshops)*, pages 1–6, 2021.

60. Attenuation by atmospheric gases and related effects. *International Telecommunication Union*, P.676-12, 2019.

61. Reference standard atmospheres. *International Telecommunication Union*, P.835-6, 2017.

62. NASA Small Spacecraft Systems Virtual Institute. Small Spacecraft Technology State of the Art. Technical report, NASA, February 2024. Accessed: 2025-05-21.

63. Picosats. RadioSat K/Ka-band, 2025. Accessed: 2025-05-21.

64. AAC Clyde Space. PULSAR-XTX High-Speed X-Band Downlink Transceiver, 2021. Accessed: 2025-05-21.

65. Tethers Unlimited, Inc. SWIFT-KTX High-Speed Ka-Band Transmitter, 2025. Accessed: 2025-05-21.

66. Priyangshu Sen, Dimitris A. Pados, Stella N. Batalama, Erik Einarsson, Jonathan P. Bird, and Josep M. Jornet. The TeraNova platform: An integrated testbed for ultra-broadband wireless communications at true Terahertz frequencies. *Computer Networks*, 179:107370, 10 2020.

67. NASA Goddard Space Flight Center. TBIRD: TeraByte InfraRed Delivery System, October 2017. Accessed: 2025-05-21.

68. Danielle Sempsrott. NASA Announces Selection of Candidates for CubeSat Space Missions, March 2023. Accessed: August 2023.